

UKAEA-CCFE-PR(20)101

M. Sasaki, T. Kobayashi, R. O. Dendy, Y. Kawachi, H.
Arakawa, S. Inagaki

Evaluation of abrupt energy transfer among turbulent plasma structures using singular value decomposition

Enquiries about copyright and reproduction should in the first instance be addressed to the UKAEA Publications Officer, Culham Science Centre, Building K1/O/83 Abingdon, Oxfordshire, OX14 3DB, UK. The United Kingdom Atomic Energy Authority is the copyright holder.

The contents of this document and all other UKAEA Preprints, Reports and Conference Papers are available to view online free at scientific-publications.ukaea.uk/

Evaluation of abrupt energy transfer among turbulent plasma structures using singular value decomposition

M. Sasaki, T. Kobayashi, R. O. Dendy, Y. Kawachi, H. Arakawa, S. Inagaki

Evaluation of abrupt energy transfer among turbulent plasma structures using singular value decomposition

M. Sasaki^{1,2,3}, T. Kobayashi⁴, R. O. Dendy^{2,3,5}, Y. Kawachi⁶,
H. Arakawa⁷, S. Inagaki^{1,2}

¹Research Institute for Applied Mechanics, Kyushu University, Kasuga 816-8580, Japan

²Research Center for Plasma Turbulence, Kyushu University, Kasuga 816-8580, Japan

³Centre for Fusion, Space and Astrophysics, Department of Physics, Warwick University, Coventry CV4 7AL, United Kingdom

⁴National Institute for Fusion Science, Toki 509-5292, Japan

⁵CCFE, Culham Science Centre, Abingdon, Oxfordshire OX14 3DB, United Kingdom

⁶Interdisciplinary Graduate School of Engineering Sciences, Kyushu University, Kasuga 816-8580, Japan

⁷Institute of Science and Engineering, Academic Assembly, Shimane University, Matsue 690-8504, Japan

E-mail: sasaki@riam.kyushu-u.ac.jp

Abstract. A method to quantify the energy transfer among turbulent structures using singular value decomposition (SVD) is presented. We apply the method to numerical turbulence data obtained from a global plasma simulation using the Hasegawa-Wakatani fluid model, in which the Kelvin-Helmholtz instability plays a dominant role. Using the SVD method, the electrostatic potential is decomposed into a background potential deformation, a zonal flow, a coherent mode and an intermittent structure. Thus there are four key structures, as distinct from the three found in conventional theory. The kinetic energy of each structure is evaluated, and the limit cycle among them is obtained. In the limit cycle, an abrupt change of the background is found to be synchronised with the period of the zonal flow. The energy transfer function of each turbulence structure, which is defined on the basis of a vorticity equation, is evaluated. This then provides physical understanding of how the limit cycle is sustained by dynamical changes in the energy transfer among structures over the its period. In addition, it is shown that the abrupt deformation of the background is caused by the nonlinear coupling between the coherent mode and the intermittent structure.

1. Introduction

Magnetically confined plasmas are nonequilibrium open systems, in which nonlinear structures are observed to arise spontaneously on the largest accessible scales. These structures typically feed on microturbulence [1], and include zonal flows [2], bulk intrinsic toroidal rotation [3], and transport barriers that can arise both within the plasma [4] and at its boundary [5]. This phenomenology is of great practical importance, because the transport of energy, momentum and particles across the plasma is conditioned by, and self-consistent with, the excitation and continuing existence of the largescale nonlinear structures [6]; the latter are often referred to as secondary structures, to distinguish them from the primary microturbulence. Understanding and predicting this phenomenology, and its consequences for the local and global behaviour of the plasma, is greatly assisted if techniques applicable to low-dimensional dynamical systems [7] can be deployed. This approach requires quantitative spatio-temporal characterisation of the salient nonlinear structures and of the microturbulence, together with the couplings between them.

A pre-requisite for this approach is to have a reliable means to identify such structures, by extracting them from experimental data and from the outputs of large-scale numerical simulations. Indeed it can be a non-trivial task to determine how many distinguishable nonlinear structures are present. This is important both for quantitative characterisation of the data, and to motivate or validate the adoption of low-dimensional analytical models in the predator-prey genre for turbulence phenomenology, see for example Refs.[2], [8]-[12]. Notable current methods include singular value decomposition (SVD) [13]-[17] and dynamical mode decomposition (DMD) [18, 19, 20]. These methods have been widely applied in plasma physics, for example to the extraction of fluid turbulent structures [21] and the visualization of phase space structures [22]. In the DMD method, the time evolution is assumed to be exponential, hence the computational cost is low. However, while the exponential assumption can work well to characterise system dynamics over relatively short timescales, beginning at any instant, it is not well adapted to system dynamics that incorporate limit cycle oscillations (LCOs) [23], which are a focus of the present paper. In plasma physics, LCOs are often observed near the threshold for local or global transitions that may also involve structure formation. Examples span electric field pulsations [24], phenomenology near the threshold for L-H transitions in global energy confinement [25, 26, 27], and edge localized modes [28]. These LCOs may significantly affect overall plasma performance, so that understanding their underlying physics is important. While the assumption of exponential time dependence in DMD treatments can be mitigated to some extent [18], DMD is not well adapted to LCOs where, as in the present paper, there is a cyclic rise and fall in the intensity of turbulence, of turbulence-driven structures, and of the coupling between them.

On the other hand, the SVD method makes no prior assumption regarding time evolution, so that the extraction of, for example, frequency chirping and phase modulation becomes possible. SVD is based on functional decomposition with respect

to orthogonal basis functions which are, by construction, uncoupled to each other. This greatly assists the evaluation of the intrinsically nonlinear forces and fluxes, which are expressed in relation to the decomposed structures, and which drive the fluctuations.

Here we apply the SVD method to a dataset obtained from a specific global simulation [29] of a magnetised cylindrical plasma based on the nonlinear Hasegawa-Wakatani coupled two-fluid model [30] for density and electrostatic potential. In this simulation, it has been found [29] that LCOs arise spontaneously, with phenomenology dominated by the Kelvin-Helmholtz (KH) instability [31]. Using the SVD method, the electrostatic potential is decomposed into the background flow, the zonal flow, a coherent mode, and an intermittent structure. We find that the LCO between these turbulent structures is synchronised with the periodicity of the zonal flow, and involves an abrupt change in the background flow. An energy transfer function based on the vorticity equation is introduced. This enables us to evaluate the cyclic dynamics of how the energy transfer among the turbulent structures changes during the LCO. The rest of the paper is organised as follows. Section 2 introduces the simulation dataset used in this study. In section 3, we describe how SVD is used to extract the spatiotemporal pattern of the turbulence. The dynamics of the energy transfer among the structures is evaluated in section 4. A summary is given in section 5.

2. Abrupt change of background and turbulence

We first introduce the dataset to which the SVD method will be applied. It relates to turbulent phenomena that arise in a global fluid simulation of a magnetised cylindrical plasma, based on the Hasegawa-Wakatani model [32]. The magnetic field, which is in the axial direction, is spatially uniform and constant. A radially inhomogeneous background flow is driven by introducing a vorticity source, such that the plasma is linearly unstable against the KH instability. The fully nonlinear evolution of the KH instability is captured by the simulation. In cases with a weak vorticity source, stationary nonlinear saturation is obtained. Above a certain threshold for the intensity of the vorticity source, LCO occurs [29], and we focus on this regime in the present study.

Figure 1(a) shows a snapshot of the fluctuating component of the electrostatic potential. Noting that the electrostatic potential is intrinsically related to the $E \times B$ bulk plasma flow, hereafter we use the terms potential or flow interchangeably, depending on the context. Here the fluctuation is translationally invariant along the axis of the cylinder; with respect to azimuthal angle, the component $m = 1$ is dominant, where m is the azimuthal mode number. This is characteristic of the nonlinear KH instability in the scenario considered [31]. The spatial pattern is dynamically modulated under the LCO, whose period is much longer than that of azimuthal rotation; further detail is given in Ref. [29]. Figure. 1(b) shows radial profiles of the magnitude of the electrostatic potential, from the axis of the cylinder to the plasma boundary. In this point, the potential is zonally averaged, meaning that its average is taken azimuthally and axially.

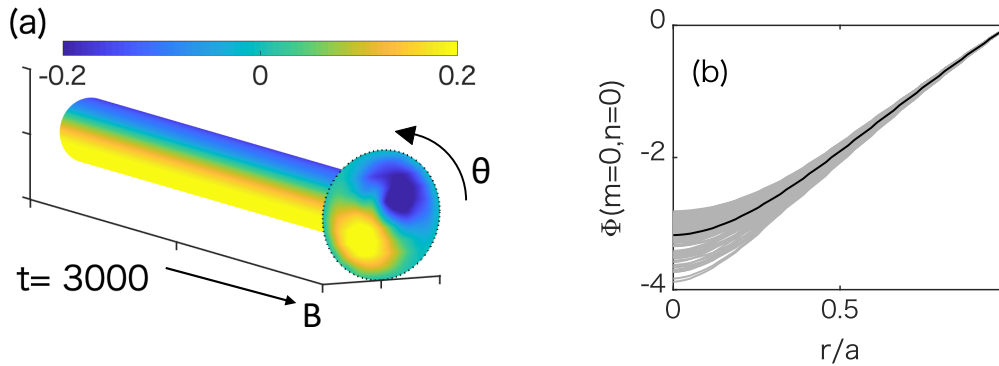


Figure 1. (a) Snapshot of three dimensional pattern of the electrostatic potential fluctuation at $t = 3000$. (b) Radial profile of the electrostatic potential with $m = n = 0$, where m and n are the azimuthal and axial mode numbers, respectively. The black line is the time averaged profile, and the gray lines show the instantaneous profiles at each time from $t = 3000$ to 4000 .

The grey lines plot instantaneous profiles at times from $t = 3000$ to $t = 4000$, with a time step of unity; here time is normalised by the ion gyro-frequency. The black line delineates the corresponding time-averaged profile. It is evident that the magnitude of the variation of the potential under the LCO is approximately 30%.

Figure 2(a) shows the time evolution of a Fourier power spectrum with respect to azimuthal modes of the electrostatic potential. The mode spectrum for azimuthal modes up to $m = 15$ shows that the LCO has a period $T_{period} \sim 150$. To further illustrate the temporal dynamics of the background potential, we construct an empirical instantaneous growth rate from the simulations, using the definition $\gamma(t) = \partial_t \ln E_{0,0}$, where $E_{0,0}$ is the kinetic energy of the background flow, calculated from the background potential. That is, $E_{0,0} = \int |\nabla_{\perp} \langle \phi \rangle|^2 d^3x$, where $\langle \cdot \cdot \cdot \rangle$ denotes the zonal average. The time evolution of $\gamma(t)$ is plotted in Fig. 2(b), showing a sequence of rapidly rising spikes which are characteristic of this type of abrupt phenomenon [33].

3. Evaluation of energy transfer by SVD

Let us now apply the SVD method to the dataset described in the previous section, so as to extract the dominant spatiotemporal structures and evaluate the energy transfer among them. We shall also examine the physical origin of the abrupt increases of the background flow noted in Fig.2, and identify the role of each structure in the LCO.

Because the KH turbulence is purely two-dimensional, we analyse the electrostatic potential $\phi(r, \theta, t)$; here $\phi(r, \theta, t)$ includes both the fluctuations and the background deformation. Using the SVD method, $\phi(r, \theta, t)$ is decomposed as

$$\phi(r, \theta, t) = \sum_j s_j \Psi_j(r, \theta) h_j(t), \quad (1)$$

Here, in relation to the j th mode: $\Psi_j(r, \theta)$ describes the mode's spatial structure; $h_j(t)$ captures its temporal evolution; and s_j is its singular value, that is, the weight

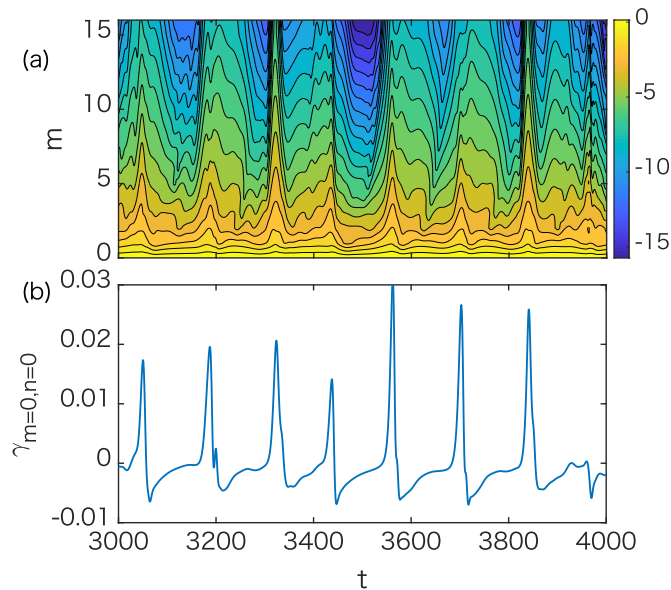


Figure 2. Time evolution of: (a) the azimuthal mode number spectrum of the electrostatic potential; (b) the empirical instantaneous growth rate of the kinetic energy of the background flow, $\gamma_{m=0,n=0} = \partial_t \ln E_{0,0}$.

that defines the relative importance [13] of the mode's contribution to $\phi(r, \theta, t)$. We emphasise that the functional form of each Ψ_j is entirely dictated *a posteriori* by the simulation outputs, without any prior assumptions. Figure 3 shows the dominant structure functions Ψ_j . These are the top nine modes, in descending order of their singular values s_j . We note that the two-dimensional pattern of $\phi(r, \theta, t)$ dynamically changes in time, as shown in Fig. 2 for Fourier space, or Fig. 1 of [18] for real space. The nine spatial structure functions shown in the left panel of Fig.3 capture background profile deformation (modes 1 and 4) and turbulent structures and fluctuations (the remaining modes). Here the mode ID numbers 1, 2, \dots 9 are in descending order of the singular values s_j . These are the dominant modes in this SVD, as can be seen from the right panel of Fig. 3, where values of s_j are plotted on a logarithmic scale for modes up to the twentieth. In the present study, we truncate the SVD modes at the ninth, for which the singular value s_9 is around 10% of the maximum value s_1 . This keeps the demand on computational resources manageable.

One can see from Fig. 3 that there are several paired modes whose spatial structures are similar and whose singular values are nearly the same, which differ only in their phase. Examples of paired modes are: ID=2, 3, ID=5, 6, and ID=7, 8. These are complex conjugate pairs, which in combination represent the azimuthal propagation, akin to the combination of sine and cosine components in Fourier mode decomposition. Thus, the summation of the pair should be treated as a single structure. There are also unpaired modes, for example modes ID=1 and ID=4, which are almost azimuthally homogeneous and do not propagate in the azimuthal direction. We wish to capture

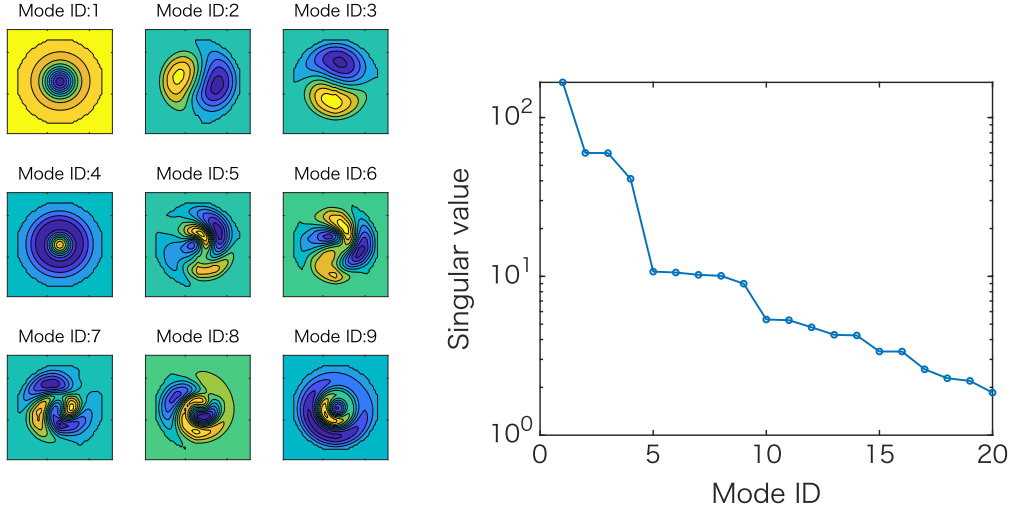


Figure 3. (Left panel) The spatial character of the nine SVD modes that have the largest singular values. (Right panel) Singular values of the first twenty SVD modes, plotted on a logarithmic scale.

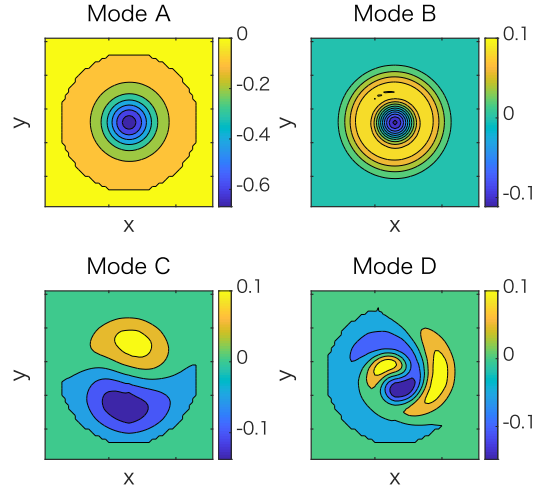


Figure 4. Dominant turbulent structures extracted by summation and truncation of the modes in Fig. 3. Mode A is invariant against azimuthal rotation, and the dominant component of Mode B is an azimuthally symmetric zonal pattern. Modes C and D are the turbulent structures.

low-dimensional phenomenology wherever possible, and therefore choose to reduce the number of degrees of freedom by taking a summation from mode ID=5 to ID=8, whose singular values are similar; we then treat the resulting summed entity as a single structure.

The spatiotemporal behaviour of the electrostatic potential is thus decomposed into four structures, $\phi_A, \phi_B, \phi_C, \phi_D$, which are defined as follows:

$$\phi(r, \theta, t) \approx \sum_{\zeta=A \sim D} \phi_{\zeta}(r, \theta, t), \quad (2a)$$

$$\phi_A(r, \theta, t) = \varphi_1(r, \theta, t), \quad (2b)$$

$$\phi_B(r, \theta, t) = \varphi_4(r, \theta, t) \quad (2c)$$

$$\phi_C(r, \theta, t) = \varphi_2(r, \theta, t) + \varphi_3(r, \theta, t), \quad (2d)$$

$$\phi_D(r, \theta, t) = \sum_{j=5}^8 \varphi_j(r, \theta, t), \quad (2e)$$

where $\varphi_j(r, \theta, t) = s_j \Psi_j(r, \theta) h_j(t)$. Snapshots of each of these four structures at $t = 3200$ are shown in Fig. 4. Mode A corresponds to the background potential deformation; mode B to the zonal flow; mode C to the coherent KH mode; and mode D to the intermittent structure. We refer to these as extracted structures of the electrostatic potential. The kinetic energy of each structure, E_ζ can be evaluated from the definition

$$E_\zeta = \frac{1}{2} \int |\nabla_\perp \phi_\zeta|^2 d^3x, \quad (\zeta = A \sim D). \quad (3)$$

The time evolution of the kinetic energy of each structure is illustrated in Fig. 5(a). Information about the relative phase of the time-evolving kinetic energy in pairs of modes can also be inferred from the phase plots in the right panel of Fig.5. The process for constructing these plots is identical to that for Lissajous figures. While, strictly, the latter term applies to superimposed simple harmonic motions, we use it more colloquially here and in Figs. 8 and 9. Lissajous figures (in this sense) are widely used to characterise strongly nonlinear structures in plasmas, see for example the treatment of heat pulse propagation in the LHD heliotron-stellarator in Figs.1,3,5,6 and 7 of Ref.[34] and Fig.7 of Ref.[35].

The behaviour of the energy that is evident in Fig. 5 is similar to that extracted by using the DMD method, see in particular Figs. 4 of Ref.[18]. The background potential (mode A) and the coherent KH mode C compete with each other. When the magnitude of mode C increases to a certain threshold, the zonal flow mode B is excited together with the intermittent structure mode D. After the appearance of modes B and D, mode C decreases and mode A increases. This cycle then repeats - it is an LCO. The period of the LCO is synchronised with the zonal flow oscillation. The time evolution of the local value of the zonal potential (mode B) at different radial locations is plotted in Fig. 5(b). The phase of mode B at $r/a = 0.16$ is the reverse of the phase at $r/a = 0.8$. The plot of the time-evolution of the potential at these two radial locations exhibits standing-wave-like structure. Successive zero-crossings - that is, phase reversal events - are synchronous with successive cycles of the LCO, where the frequencies of the LCO and the zonal flow are similar and the phase relation between the zonal flow and the LCO does not vary over time. The zonal flow mode B always peaks sharply just before each abrupt increase of the background flow mode A, and the phase of mode B reverses after the burst of mode A.

4. Energy transfer dynamics among SVD modes

The energy transfer among the structures extracted in the preceding section can be characterised in terms of an energy transfer function that is based on the vorticity

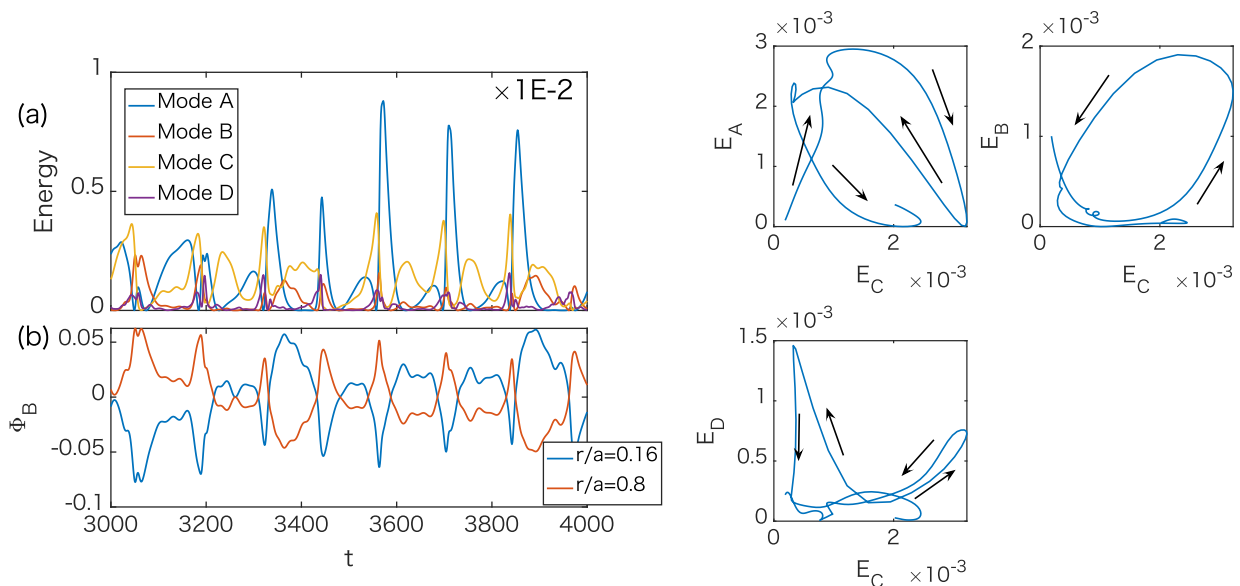


Figure 5. Characterising limit cycle oscillations. Left panel. Time evolution of: (a) the kinetic energy of each of the four structures A to D identified in Fig. 4; (b) the local values of the zonal flow potential (Mode B) at widely separated radial locations $r/a = 0.16$ and 0.8 , at angular position $\theta = 0$. Right panel. Three Lissajous figures plotting the time evolution of the kinetic energy of the three Modes A, B and D against that of Mode C, during the time interval $3080 < t < 3250$. The arrows show the direction of time evolution.

equation, as follows. The vorticity equation is

$$\partial_t \nabla_{\perp}^2 \phi = - [\phi, \nabla_{\perp}^2 \phi] - \nu \nabla_{\perp}^2 \phi + S, \quad (4)$$

Here the first term on the RHS is the convective derivative, defined as $[\phi, \nabla_{\perp}^2 \phi] = r^{-1} (\partial_r \phi \partial_{\theta} \nabla_{\perp}^2 \phi - \partial_r \nabla_{\perp}^2 \phi \partial_{\theta} \phi)$, and ν and S are the ion-neutral collision frequency and the vorticity source, respectively. The kinetic energy evolution equation can be derived by multiplying both sides of Eq. (4) by ϕ and performing a spatial integration. Here, ϕ is decomposed into the SVD structures from mode A to mode D as in Eq. (2a). The kinetic energy of Mode ζ can be written as ($\zeta = A \sim D$)

$$\partial_t E_{\zeta} = \sum_{\alpha, \beta=A \sim D} J(\zeta|\alpha, \beta) - 2\nu E_{\zeta} - \int \phi_{\zeta} S d^3x, \quad (5a)$$

$$J(\zeta|\alpha, \beta) = \int \phi_{\zeta} [\phi_{\alpha}, \nabla_{\perp}^2 \phi_{\beta}] d^3x, \quad (5b)$$

where the square brackets in Eq. (5b) denote the convective derivative as defined following Eq. (4). The energy transfer function, $J(\zeta|\alpha, \beta)$, quantifies the energy flow to the mode labelled ζ that arises from nonlinear coupling between the modes labelled α and β . Positive (or negative) $J(\zeta|\alpha, \beta)$ contributes to driving (or damping). The terms in the RHS of Eq. (5a) are linear, except for the energy transfer term. In the present SVD context, Eq. (5a) can be viewed as a natural extension of the energy transfer equation in Fourier space [36, 37]. It is well adapted to understanding the energy interaction among the turbulent structures identified using SVD, which contain multiple

Fourier components. In the absence of such structures, a Fourier-based approach to energy transfer would suffice for zonal flows, which can be described by a single Fourier component. It follows that the evidently nonlinear features of the system dynamics, for example those shown in Fig. 5, must stem from the energy transfer among the turbulent structures. In order to understand the underlying physics of the system, it is therefore necessary to examine the behaviour of the energy transfer function in greater detail. As a preliminary, we note that $J(\zeta|\alpha, \beta)$ is not symmetric with respect to α and β . Given the four structures A to D, there are thus sixteen relevant mode pairings. Table 1 specifies how we label ("Coupling ID") these pairings using the first sixteen integers. We note that the SVD method does not involve well-defined matching criteria with respect to frequency or wavenumber because, in general, SVD modes contain multiple Fourier modes. In the present paper, mode D is a good example of this.

Figure 6 seeks to capture the temporal variation of $J(\zeta|\alpha, \beta)$ for each structure A to D, resulting from each of the sixteen coupling combinations, from two different perspectives. The four left panels, Fig. 6 (a)-(d), plot the instantaneous values that are taken by each $J(\zeta|\alpha, \beta)$ at each unit time-step during the interval $3000 < t < 4000$ which was also considered in Figs. 2, and 5. For example, Fig. 6(c) shows that for mode C, the four sources/sinks of nonlinear drive that contribute most strongly to energy transfer (both positive and negative) are the mode pairings with coupling ID = 4, 8, 13 and 14. From Table 1, in (α, β) terms, these pairings are (A,D), (B,D), (D,A) and (D,B). Conversely, from Fig. 6(b) it is evident that energy transfer to and from mode B is dominated by the mode pairing with coupling ID = 12, 15, 16 that are $(\alpha, \beta) = (C, D), (D, C), (D, D)$. From Fig. 6(a), one can see that the background flow, mode A, is affected primarily by the self-couplings (C,C) and (D,D) and by the pair couplings (C,D) and (D,C). We note from Fig. 4 that the azimuthally symmetric background flow is contained in mode A and partly in mode B. This flow is driven by the vorticity source. It follows that net negative nonlinear energy transfer to mode A acts to relax the background flow. In contrast, for mode C and mode D, nonlinear damping due to self-coupling is found to be weak, in that the contributions from the coupling ID=11 for mode C and 16 for mode D are small. The four right panels, Fig. 6(e)-(h), plot the explicit time evolution of $J(\zeta|\alpha, \beta)$ on a colour scale, for the four modes (one panel per mode) in relation to the sixteen mode pairings. The energy transfers among the structures are strongly non-time-stationary: the discrete bursts of activity correlate necessarily with those in Fig. 5, which align with the LCO period, as discussed previously.

The energy transfer functions for each structure during a single LCO period, $3120 < t < 3220$, are illustrated in Fig. 7, where only the most important couplings are shown. There are three phases, because the energy flow pattern changes significantly between the first half ($3120 < t < 3180$), the middle regime ($t \sim 3190$), and the second half ($3200 < t < 3220$). This pattern corresponds to the growth, saturation and damping of the zonal flow, mode B. The energy transfer to the zonal flow changes its sign at $t \sim 3190$, at which time the zonal flow peaks in energy. Simultaneously, there

is an abrupt onset to the nonlinear drive of the background flow (mode A), due to the coupling with mode C and mode D, see Fig. 7(c); the energy of mode A, previously decaying, starts to increase.

The x -axis of all three panels of Fig. 8 is $J(C|A, C)$. This is chosen because, in general, $J(\zeta|A, \zeta)$ represents the generalised linear drive of the mode labelled ζ by the KH instability, which arises from deformation of the background potential mode A. This drive would be linear, notwithstanding its apparently nonlinear mathematical character, in an ordering scheme where mode A is zeroth order while the other modes are order-epsilon. In Fig. 8 the focus is thus on the different nonlinear drives of the coherent KH mode C, in relation to the linear drive. The linear drive for the coherent KH mode C, which corresponds to $J(C|A, C)$, changes its role in accordance with the phase of the LCO. It is apparent from Fig. 7(a) that, during the first half of the LCO, mode C obtains energy from its coupling with the background potential deformation mode A; that is, mode C is linearly destabilized by the flow inhomogeneity. This phase of the LCO ends at $t \sim 3185$ in Fig. 7, and this determines the parameter t_2 which is used throughout Figs. 8 and 9 to denote the end of the first half (blue trace) of the LCO cycle. Thereafter, Fig. 8(a) shows that coupling $J(C|B, C)$ of the KH mode C with the zonal flow mode B acts to suppress mode C; this is a back reaction which drives the zonal flow. In the Lissajous figures (Figs. 8 and 9), the system trajectory during the three time intervals $3080 < t < 3185$, $3185 < t < 3195$ and $3195 < t < 3250$ is plotted using blue, red and black lines, respectively. The nonlinear drive of mode C by its coupling with the intermittent structure mode D, characterised by $J(C|C, D)$ in Fig. 8(b), rises abruptly when the linear drive becomes large, that is $J(C|A, C) \sim 0.2$ in the blue phase. The steady decline of $J(C|A, C)$ thereafter, through zero and down to -0.2 , results in a second surge in the value of $J(C|C, D)$ during the middle phase of the LCO (red trace), and an equally abrupt decline during the second half (black trace). The plot of $J(C|D, D)$ in Fig. 8(c) shows that the nonlinear self-interaction of mode D does not contribute significantly to the drive of mode C during the first half of the LCO (blue trace). Thereafter its abrupt rise and fall takes place in parallel with that of $J(C|C, D)$, with similar magnitude.

The linear drive for the intermittent structure mode D corresponds to $J(D|A, D)$. The Lissajous figures for $J(D|\alpha, \beta)$ during the LCO are shown in Fig. 9, and demonstrate that $J(D|A, D)$ changes its role in accordance with the phase of the LCO, like $J(C|A, C)$ in Fig. 8 [18]. Figure 9(a) shows that for mode D, unlike for mode C, the deformation of the KH mode C due to its nonlinear coupling with the background flow mode A contributes to the drive. Deformation of mode C by the zonal flow B also affects the energy transfer to Mode D, as can be inferred from Fig. 9(b). This shows a rather abrupt reversal between the first half (blue trace) and second half (red, then black, traces) of the LCO, giving rise to a well-defined figure-8. The nonlinear coupling of Mode D with the zonal flow mode B is shown in Fig. 9(c). The sign of $J(D|B, D)$ is always negative, implying that it contributes to the suppression of mode D throughout the LCO. As seen in the Lissajous figure for $J(D|C, D)$ in Fig. 9(d), nonlinear coupling

with mode C drives mode D during the first half (blue trace) of the LCO; damps it during the middle phase (red trace) and much of the final phase (black trace); while contributing a small drive near the end of the LCO.

The energy flow patterns inferred from Figs. 8 and 9 during a single LCO period are summarized in Fig. 10. We have found that important roles in the sustainment of the LCO are played by the secondary structures, namely the zonal flow mode B and the intermittent structure mode D, notably through their nonlinear coupling with the KH mode C.

We now perform a quantitative check on our inference that the abrupt energy input to the background flow mode A at $3185 < t < 3195$ causes the abrupt increase in the background flow that is shown in Fig. 2. Dividing both sides of Eq. (5a) by E_C , an equation for the time constant of mode A, γ_A , can be formally derived as

$$\gamma_A = E_A^{-1} \sum_{\alpha, \beta} J(A|\alpha, \beta) - \nu. \quad (6)$$

From Fig. 2, the time constant at the abrupt increase can be estimated as $\gamma_A \sim 2 \times 10^{-2} \gg \nu = 5 \times 10^{-3}$. This value can be explained as $E_A^{-1} \sum_{\alpha, \beta} J(A|\alpha, \beta) \sim 2.5 \times 10^{-2}$, where we use $E_A = 2 \times 10^{-3}$ and $\sum_{\alpha, \beta} J(A|\alpha, \beta) \approx J(A|C, D) \sim 5 \times 10^{-5}$. This tends to confirm that the abrupt increase of the background flow mode A is realised by the nonlinear coupling between the coherent KH mode C and the nonlinearly driven intermittent structure D. We note that a strong role for the zonal flow mode B in the abrupt change of the background flow is also implicit. This is because, as we have already shown, deformation of modes C and D by mode B abruptly alters the characteristics of nonlinear energy transfer involving modes C and D.

5. Discussion and Conclusions

Using the SVD method, the global phenomenology of the simulated turbulent plasma has been converted into a low-dimensional dynamical system. The electrostatic potential is decomposed into four elements, which are apparently the minimal set: the deformation of the background; the zonal flow; the coherent KH mode; and the intermittent structure. The kinetic energy content of these four modes is found to exhibit an LCO, in which an abrupt change of the background potential is synchronized with the zonal flow period.

The SVD approach has enabled us to quantify the multiple nonlinear energy flows that underly this LCO. We first construct and evaluate the energy transfer function for each turbulence structure, based on a vorticity equation. This then provides physical understanding of how the LCO is sustained by dynamical changes in the energy transfer among structures over the LCO period. In summary, coupling between the coherent mode and the intermittent structure drives the zonal flow, which provides resilience for the background potential, which causes the abrupt deformation of the background.

In some previous theoretical approaches, the LCO considered here is often described in terms of a predator-prey model [9] that involves only three elements, namely the background, the zonal flow and microturbulence. Thus, the results in the present paper

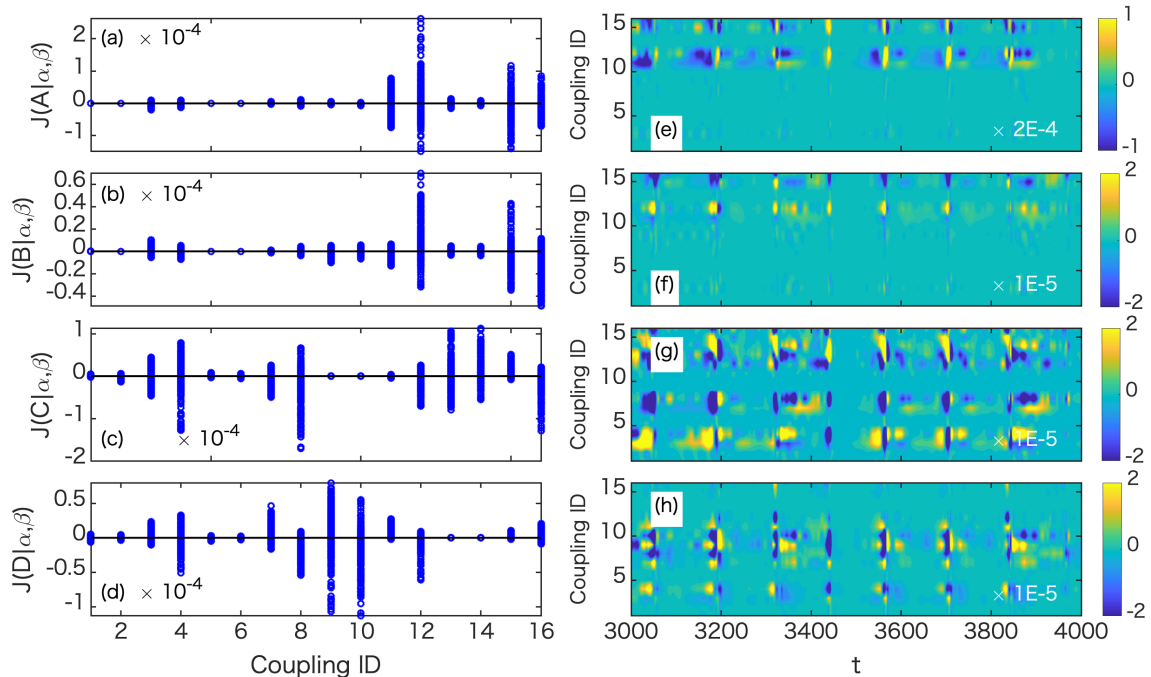


Figure 6. (a)-(d): Time variation of the energy transfer functions for each structure. (e)-(h): Temporal evolution of the energy transfer functions for each structure, where (e) $J(A|\alpha, \beta)$, (h) $J(B|\alpha, \beta)$, (g) $J(C|\alpha, \beta)$, and (h) $J(D|\alpha, \beta)$, where $\alpha + \beta$ denotes the coupling between mode α and mode β , in the order corresponding to Eq.(5b).

imply that this conventional model is incomplete. Furthermore, we have found that the hitherto neglected intermittent structure plays crucial roles in the dynamics of the system. The important role of the intermittent structure in the abrupt change in transport has also been identified experimentally [38].

In addition, we have found that the zonal flow oscillation is synchronised with the LCO. The physical mechanism that determines the frequency of the zonal flow remains an unresolved theoretical issue. In the context of the present work, we note that in basic experiments, the excitation of an intermittent structure, referred to as "splash", has been observed to be synchronized with the zonal flow oscillation [39, 40]. This tendency is similar to the behaviour of the intermittent mode D in the present study. This motivates our conjecture that the generation and annihilation of the intermittent structure, together with the deformation of the background flow, may determine the frequency of the zonal flow.

In conclusion, the SVD approach has provided significant new physical insights into the phenomenology of this classical nonlinear KH plasma system.

Acknowledgements

This work was partly supported by a grant-in-aid for scientific research of JSPS, Japan

Coupling ID	Combination of structures
1	$A + A$
2	$A + B$
3	$A + C$
4	$A + D$
5	$B + A$
6	$B + B$
7	$B + C$
8	$B + D$
9	$C + A$
10	$C + B$
11	$C + C$
12	$C + D$
13	$D + A$
14	$D + B$
15	$D + C$
16	$D + D$

Table 1. List of coupling IDs. Each number denotes the combination of structures which contribute to the coupling.

(16K18335, 17H06089, 16H02442, 15H02155, 15H02335, 18K03578), the collaboration programs of NIFS (NIFS17KNST122, NIFS18KNST137), Asada Science Foundation, Progress 100 of Kyushu University (NB80645028), and the RIAM of Kyushu University. This work was carried out partly within the framework of the EUROfusion Consortium and has received funding from the Euratom research and training programme 2014-2018 and 2019-2020 under grant agreement No 633053. The work received support from the RCUK Energy Programme grant no. EP/T012250/1. The views and opinions expressed herein do not necessarily reflect those of the European Commission.

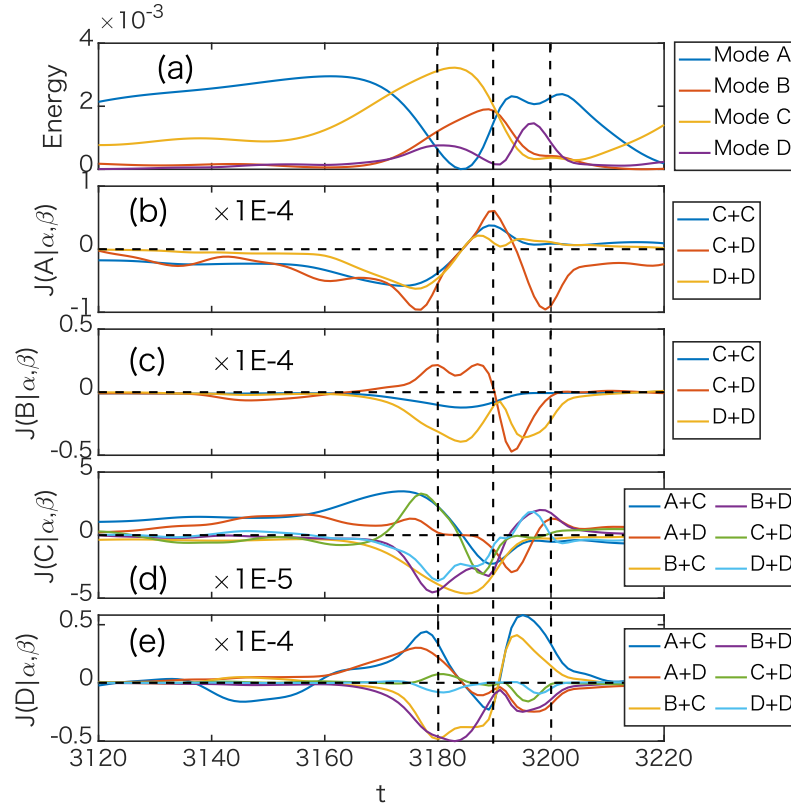


Figure 7. Time evolution of (a) kinetic energy and (b)-(e) energy transfer function for each structure. Only the energy transfer functions for the most important nonlinear couplings are shown.

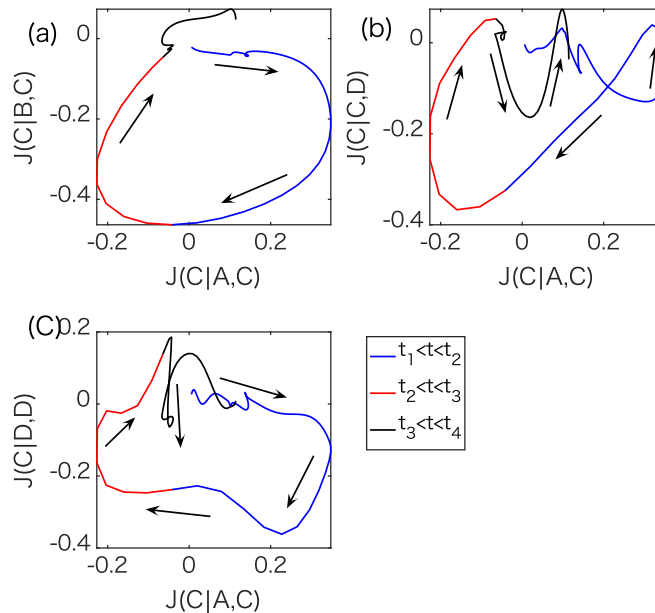


Figure 8. Lissajous figures for the three dominant energy transfer functions for the KH mode C, $J(C|\alpha,\beta)$, where the arrows show the direction of the time-evolution. Here, $t_1 = 3080$, $t_2 = 3185$, $t_3 = 3195$ and $t_4 = 3250$.

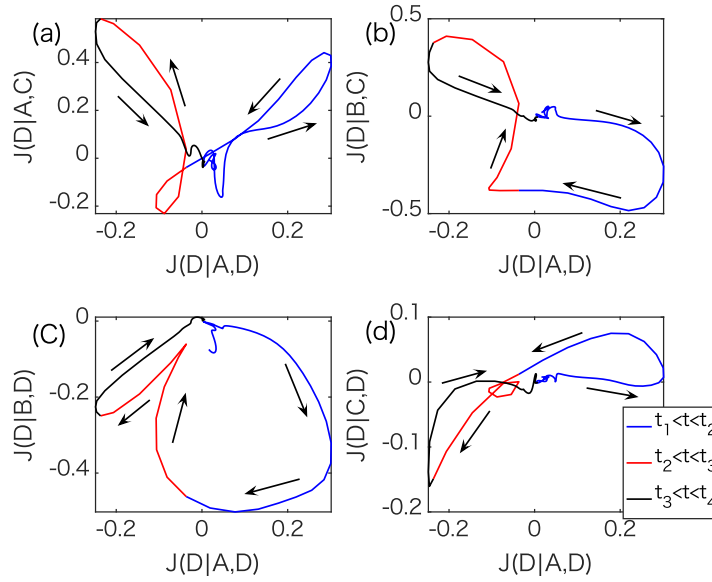


Figure 9. Lissajous figures for the four dominant energy transfer function for the intermittent mode D, $J(D|\alpha, \beta)$, where the arrows show the direction of the evolution. Here, $t_1 = 3080, t_2 = 3185, t_3 = 3195$ and $t_4 = 3250$.

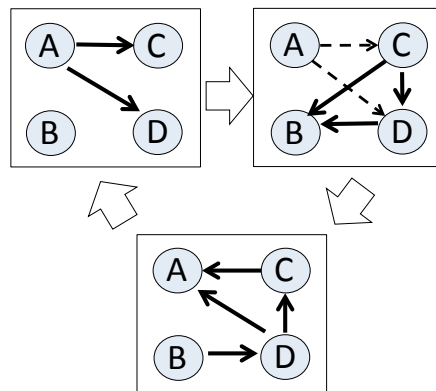


Figure 10. Schematic view of the energy flow among turbulent structures during the limit cycle oscillation, where A-D in the circles denote the Mode A-D, respectively, and the arrows show the directions of the energy flow. The pattern of the energy flow changes during one period of the LCO.

Reference

- [1] Sanae-I Itoh. Structure formation in turbulent plasmas. *Plasma and Fusion Research*, 4:038–038, 2009.
- [2] Patrick H Diamond, SI Itoh, K Itoh, and TS Hahm. Zonal flows in plasma—a review. *Plasma Physics and Controlled Fusion*, 47(5):R35, 2005.
- [3] ÖD Gürcan, PH Diamond, TS Hahm, and R Singh. Intrinsic rotation and electric field shear. *Physics of Plasmas*, 14(4):042306, 2007.
- [4] X Litaudon. Internal transport barriers: critical physics issues? *Plasma Physics and Controlled Fusion*, 48(5A):A1, 2006.
- [5] Fritz Wagner. A quarter-century of h-mode studies. *Plasma Physics and Controlled Fusion*, 49(12B):B1, 2007.
- [6] Hamed Biglari, PH Diamond, and PW Terry. Influence of sheared poloidal rotation on edge turbulence. *Physics of Fluids B: Plasma Physics*, 2(1):1–4, 1990.
- [7] H Imamura. Introduction to nonlinear analysis for engineerings, suurikougakusha-sha co.,ltd. *Applied Mathematics*, 16(2):185–186, 2006.
- [8] K Miki, PH Diamond, S-H Hahn, WW Xiao, Özgür D Gürcan, and GR Tynan. Physics of stimulated $l \rightarrow h$ transitions. *Physical Review Letters*, 110(19):195002, 2013.
- [9] Eun-jin Kim and PH Diamond. Zonal flows and transient dynamics of the l - h transition. *Physical Review Letters*, 90(18):185006, 2003.
- [10] K Itoh, K Hallatschek, S-I Itoh, PH Diamond, and S Toda. Coherent structure of zonal flow and onset of turbulent transport. *Physics of Plasmas*, 12(6):062303, 2005.
- [11] SI Itoh and K Itoh. A mini–max principle for drift waves and mesoscale fluctuations. *Plasma Physics and Controlled Fusion*, 53(1):015008, 2010.
- [12] Makoto Sasaki, K Itoh, S-I Itoh, and Naohiro Kasuya. Zonal flows induced by symmetry breaking with existence of geodesic acoustic modes. *Nuclear Fusion*, 52(2):023009, 2012.
- [13] T Dudok de Wit, A-L Pecquet, J-C Vallet, and R Lima. The biorthogonal decomposition as a tool for investigating fluctuations in plasmas. *Physics of Plasmas*, 1(10):3288–3300, 1994.
- [14] JS Kim, DH Edgell, JM Greene, EJ Strait, and MS Chance. MHD mode identification of tokamak plasmas from Mirnov signals. *Plasma Physics and Controlled Fusion*, 41(11):1399, 1999.
- [15] GS Xu, BN Wan, W Zhang, QW Yang, L Wang, and YZ Wen. Multiscale coherent structures in tokamak plasma turbulence. *Physics of Plasmas*, 13(10):102509, 2006.
- [16] DR Hatch, F Jenko, A Bañón Navarro, V Bratanov, PW Terry, and MJ Pueschel. Linear signatures in nonlinear gyrokinetics: interpreting turbulence with pseudospectra. *New Journal of Physics*, 18(7):075018, 2016.
- [17] DR Hatch, MJ Pueschel, F Jenko, WM Nevins, PW Terry, and H Doerk. Magnetic stochasticity and transport due to nonlinearly excited subdominant microtearing modes. *Physics of Plasmas*, 20(1):012307, 2013.
- [18] M Sasaki, Y Kawachi, RO Dendy, H Arakawa, N Kasuya, F Kin, K Yamasaki, and S Inagaki. Using dynamical mode decomposition to extract the limit cycle dynamics of modulated turbulence in a plasma simulation. *Plasma Physics and Controlled Fusion*, 61(11):112001, 2019.
- [19] Akira Kusaba, Tetsuji Kuboyama, and Shigeru Inagaki. Sparsity-promoting dynamic mode decomposition of plasma turbulence. *Plasma and Fusion Research*, 15:1301001–1301001, 2020.
- [20] Alan A Kaptanoglu, Kyle D Morgan, Chris J Hansen, and Steven L Brunton. Characterizing magnetized plasmas with dynamic mode decomposition. *Physics of Plasmas*, 27(3):032108, 2020.
- [21] Diego del Castillo-Negrete, Steven P Hirshman, Donald A Spong, and Eduardo F D ’ Azevedo. Compression of magnetohydrodynamic simulation data using singular value decomposition. *Journal of Computational Physics*, 222(1):265–286, 2007.
- [22] DR Hatch, F Jenko, A Bañón Navarro, V Bratanov, PW Terry, and MJ Pueschel. Linear signatures in nonlinear gyrokinetics: interpreting turbulence with pseudospectra. *New Journal of Physics*,

- 18(7):075018, 2016.
- [23] Yoshiki Kuramoto. *Chemical oscillations, waves, and turbulence*. Courier Corporation, 2003.
 - [24] A Fujisawa, H Iguchi, H Idei, S Kubo, K Matsuoka, S Okamura, K Tanaka, T Minami, S Ohdachi, S Morita, et al. Discovery of electric pulsation in a toroidal helical plasma. *Physical Review Letters*, 81(11):2256, 1998.
 - [25] T Kobayashi, K Itoh, T Ido, K Kamiya, S-I Itoh, Y Miura, Yoshihiko Nagashima, A Fujisawa, S Inagaki, K Ida, et al. Spatiotemporal structures of edge limit-cycle oscillation before l-to-h transition in the jft-2m tokamak. *Physical Review Letters*, 111(3):035002, 2013.
 - [26] L Schmitz, L Zeng, TL Rhodes, JC Hillesheim, EJ Doyle, RJ Groebner, WA Peebles, KH Burrell, and G Wang. Role of zonal flow predator-prey oscillations in triggering the transition to h-mode confinement. *Physical Review Letters*, 108(15):155002, 2012.
 - [27] G Birkenmeier, M Cavedon, GD Conway, P Manz, U Stroth, R Fischer, G Fuchert, T Happel, FM Laggner, M Maraschek, et al. Magnetic structure and frequency scaling of limit-cycle oscillations close to l-to h-mode transitions. *Nuclear Fusion*, 56(8):086009, 2016.
 - [28] Sanae-I Itoh, Kimitaka Itoh, Atsushi Fukuyama, and Yukitoshi Miura. Edge localized mode activity as a limit cycle in tokamak plasmas. *Physical Review Letters*, 67(18):2485, 1991.
 - [29] Makoto Sasaki, Yann Camenen, A Escarguel, S Inagaki, Naohiro Kasuya, K Itoh, and T Kobayashi. Formation of spiral structures of turbulence driven by a strong rotation in magnetically cylindrical plasmas. *Physics of Plasmas*, 26(4):042305, 2019.
 - [30] Akira Hasegawa and Masahiro Wakatani. Self-organization of electrostatic turbulence in a cylindrical plasma. *Physical Review Letters*, 59(14):1581, 1987.
 - [31] W Horton, T Tajima, and T Kamimura. Kelvin–helmholtz instability and vortices in magnetized plasma. *The Physics of Fluids*, 30(11):3485–3495, 1987.
 - [32] Makoto Sasaki, Naohiro Kasuya, K Itoh, S Toda, Takuma Yamada, Yusuke Kosuga, Yoshihiko Nagashima, T Kobayashi, H Arakawa, K Yamasaki, et al. Topological bifurcation of helical flows in magnetized plasmas with density gradient and parallel flow shear. *Physics of Plasmas*, 24(11):112103, 2017.
 - [33] K Itoh, S-I Itoh, Yusuke Kosuga, M Lesur, and T Ido. Onset condition of the subcritical geodesic acoustic mode instability in the presence of energetic-particle-driven geodesic acoustic mode. *Plasma Physics Reports*, 42(5):418–423, 2016.
 - [34] RO Dendy, SC Chapman, and S Inagaki. Modelling the measured local time evolution of strongly nonlinear heat pulses in the large helical device. *Plasma Physics and Controlled Fusion*, 55(11):115009, 2013.
 - [35] H Zhu, RO Dendy, SC Chapman, and S Inagaki. A quantitative model for heat pulse propagation across large helical device plasmas. *Physics of Plasmas*, 22(6):062308, 2015.
 - [36] P Manz, M Ramisch, and U Stroth. Physical mechanism behind zonal-flow generation in drift-wave turbulence. *Physical Review Letters*, 103(16):165004, 2009.
 - [37] Yoshihiko Nagashima, Sanae-I Itoh, Shunjiro Shinohara, Masayuki Fukao, Akihide Fujisawa, Kenichiro Terasaka, Yoshinobu Kawai, George R Tynan, Patrick H Diamond, Masatoshi Yagi, et al. Observation of the parametric-modulational instability between the drift-wave fluctuation and azimuthally symmetric sheared radial electric field oscillation in a cylindrical laboratory plasma. *Physics of Plasmas*, 16(2):020706, 2009.
 - [38] T Kobayashi, S Inagaki, M Sasaki, Y Kosuga, H Arakawa, T Yamada, Y Nagashima, Y Miwa, N Kasuya, A Fujisawa, et al. Azimuthal inhomogeneity of turbulence structure and its impact on intermittent particle transport in linear magnetized plasmas. *Physics of Plasmas*, 22(11):112301, 2015.
 - [39] H Arakawa, S Inagaki, M Sasaki, Y Kosuga, T Kobayashi, N Kasuya, Y Nagashima, T Yamada, M Lesur, A Fujisawa, et al. Eddy, drift wave and zonal flow dynamics in a linear magnetized plasma. *Scientific Reports*, 6(1):33371, 2016.
 - [40] H Arakawa, M Sasaki, S Inagaki, Y Kosuga, T Kobayashi, N Kasuya, T Yamada, Y Nagashima, F Kin, A Fujisawa, et al. Roles of solitary eddy and splash in drift wave–zonal flow system in

a linear magnetized plasma. *Physics of Plasmas*, 26(5):052305, 2019.